

PNAS

www.pnas.org

Supplementary Information for

Critical role of Aquaporin-1 and telocytes in infantile hemangioma response to propranolol beta-blockade

François Moisan^{1,*}, Sandra Oucherif¹, Priscilla Kaulanjan-Checkmodine¹, Sorilla Prey^{1,2}, Benoît Rousseau³, Marc Bonneu⁴, Stéphane Claverol⁴, Etienne Gontier⁵, Sabrina Lacomme⁵, Lea Dousset^{1,2}, Thierry Couffinhal⁶, Jerome Toutain⁷, Maya Loot⁸, Muriel Cario-André^{1,9}, Marie-Laure Jullié¹⁰, Christine Léauté-Labrèze^{1,2,9}, Alain Taieb^{1,2,9}, Hamid Reza Rezvani^{1,2,9}

François Moisan

Email: francois.moisan@u-bordeaux.fr

This PDF file includes:

Supplementary text: Methods
Figures S1 to S11
Tables S1 to S3
SI References

Supplementary Information Text

Methods:

RNA isolation and real-time reverse transcription PCR

RNA was isolated from sub-confluent growing cells using the NucleoSpin® RNA kit (MACHEREY-NAGEL, Germany) and 0.5 µg RNA was used for first-strand cDNA synthesis by using PrimeScript™ RT Master Mix (Takara, Japan) according to the manufacturer's protocols. 10x diluted cDNA was prepared and the final 20 µl reaction mixture included 300 nM of each primer and 1x Brilliant III Ultra-Fast SYBR® Green QPCR Master Mix (Agilent, USA). Initial denaturation for all PCR reactions was 3 min at 95 °C, followed by 40 cycles of PCR amplification (95 °C for 5 sec and 60 °C for 5 sec) using the CFX96 Real-Time PCR Detection System instrument (Bio-Rad, USA). The PCR product obtained by specific primers for glucuronidase beta (GUSB) was used as a reference gene to control for loading. Amplification efficiencies were determined by serial dilutions, and all reactions were performed in triplicate. Melt curves were performed after each run to confirm the primer pair specificity.

Lentivirus generation and establishment of GFP⁺ cells

The lentiviral vectors pGIPZ (TurboGFP and shRNA are part of a bicistronic transcript allowing the visual marking of shRNA-expressing cells) targeting ADRB2 or AQP1 and the non-silencing control were acquired from Thermo Fisher, USA. AQP1 overexpression was achieved by lentiviral transduction of 217EX-A4384-Lv230 ORF expression clone for AQP1 (NM_198098.3) and 217EX-NEG-Lv230 Empty control vector for pReceiver-Lv230 respectively called pAQP1 and P0 in the paper, acquired from Genecopoeia, MD, USA. Lentiviral particles expressing GFP were prepared using 293T cells plated in 175 cm² flasks. Twenty-four hours after seeding, near-confluent cells were co-transfected with 45 µg pHR2-GLF lentiviral vector together with pCMVΔR8.74 packaging and VSV-G-expressing vectors (3:2:1 ratio) in the presence of 25 µM chloroquine (Sigma-Aldrich, USA). The medium was changed after 8–12 h and then collected at 24–36 h, filtered through a 0.45 µm polyethersulfone filter, and ultracentrifuged for 2 h at 20,000 rpm at 4 °C. The viral pellet was resuspended in plain IMDM medium (Invitrogen, USA) and frozen at -80 °C. The viral titer was determined by infection of 293T cells with several dilutions of the virus and analysis of GFP⁺ cells by flow cytometry 36 h later. U87-MG cells were transduced with lentivirus. After 16–24 h incubation with virus, the medium changed. Transduced cells were selected with 1 µg/mL of puromycin for 5 days. GFP⁺ cells were sorted and purified by flow cytometry.

Protein extraction and western blotting

Cell pellets were resuspended in a lysis buffer RIPA [Tris-HCl, pH 8, 50 mM; NaCl 150 mM; sodium dodecyl sulfate 0.1%; NP40 1%; sodium deoxycholate 0.5%; protease inhibitors cocktail (Sigma)]. After 30 min on ice, the samples were centrifuged for 15 min at 15 000g. The supernatants containing soluble proteins were analyzed by western blotting: 30 micrograms of proteins were separated by 10% sodium dodecyl sulfate–polyacrylamide gel electrophoresis and transferred onto polyvinylidene difluoride membranes (Millipore), using a mini-blot wet transfer (Bio-Rad). Membranes were then blocked for 1 h in 5% skim milk in Tris-buffered saline-T (Tris-HCl, pH 7.5, 100 mM, NaCl 0.9%, Tween-20 0.05%) and incubated overnight at 4°C with primary antibody (Table S3) diluted at the appropriate concentration in blocking solution. Blots were washed three times in Tris-buffered saline-T, and then incubated for 1 h with peroxidase-conjugated secondary antibody (Table S3). After washes, signals were detected using chemiluminescence reagent (Bio-Rad).

Proteomic analysis

Proteomic analysis was performed as previously explained (1, 2).

Sample preparation and protein digestion

Samples were solubilized in Laemmli buffer and were deposited in triplicate onto SDS-PAGE. Separation was stopped once proteins had entered the resolving gel. After colloidal blue staining, bands were cut out from the SDS-PAGE gel and subsequently cut into 1 mm x 1 mm gel pieces. Gel pieces were destained in 25 mM ammonium bicarbonate 50% ACN, rinsed twice in ultrapure water and shrunk in ACN for 10 min. After removal of ACN, gel pieces were dried at room temperature, covered with the trypsin solution (10 ng/μl in 50 mM NH₄HCO₃), rehydrated at 4 °C for 10 min, and finally incubated overnight at 37 °C. Spots were then incubated for 15 min in 50 mM NH₄HCO₃ at room temperature with rotary shaking. The supernatant was collected, and an H₂O/ACN/HCOOH (47.5:47.5:5) extraction solution was added onto gel slices for 15 min. The extraction step was repeated twice. Supernatants were pooled, dried in a vacuum centrifuge, and resuspended in 25 μl of formic acid (5%, v/v) so as to inject about 500 ng.

nLC-MS/MS analysis

Peptide mixture was analysed on a Ultimate 3000 nanoLC system (Dionex, Amsterdam, The Netherlands) coupled to an Electrospray Q-Exactive quadrupole Orbitrap benchtop mass spectrometer (Thermo Fisher Scientific, San Jose, CA). Ten microliters of peptide digests were loaded onto a 300-μm-inner diameter x 5-mm C18 PepMap™ trap column (LC Packings) at a flow rate of 30 μL/min. The peptides were eluted from the trap column onto an analytical 75-mm id x 25-cm C18 Pep-Map column (LC Packings) with a 4–40% linear gradient of solvent B in 108 min (solvent A was 0.1% formic acid in 5% ACN, and solvent B was 0.1% formic acid in 80% ACN). The separation flow rate was set at 300 nL/min. The mass spectrometer operated in positive ion mode at a 1.8-kV needle voltage. Data were acquired using Xcalibur 2.2 software in a data-dependent mode. MS scans (m/z 300-2000) were recorded at a resolution of R = 70 000 (@ m/z 200) and an AGC target of 1 x 10⁶ ions was collected within 100 ms. Dynamic exclusion was set to 30 s and the top 15 ions were selected from fragmentation in HCD mode. MS/MS scans with a target value of 1 x 10⁵ ions were collected with a maximum fill time of 120 ms and a resolution of R = 35000. Additionally, only +2 and +3 charged ions were selected for fragmentation. Other settings were as follows: neither sheath nor auxiliary gas flow heated capillary temperature, 260 °C; normalized HCD collision energy of 25% and an isolation width of 3 m/z.

Database search and results processing

Data were searched by SEQUEST through Proteome Discoverer 1.4 (Thermo Fisher Scientific Inc.) against a subset of the 2018.01 version of the UniProt database restricted to the Homo Sapiens Reference Proteome Set (71,536 entries). Spectra from peptides higher than 5000 Da or lower than 350 Da were rejected. The search parameters were as follows: mass accuracy of the monoisotopic peptide precursor and peptide fragments were set to 10 ppm and 0.02 Da respectively. Only b- and y-ions were considered for mass calculation. Oxidation of methionines (+16 Da) and carbamidomethylation of cysteines (+57 Da) were considered as variable and fixed modifications, respectively. Two missed trypsin cleavages were allowed. Peptide validation was performed using the Percolator algorithm (3) and only “high confidence” peptides were retained corresponding to a 1% false positive rate at peptide level.

Label-Free Quantitative Data Analysis

Raw LC-MS/MS data were imported in Progenesis QI for Proteomics 2.0 (Nonlinear Dynamics Ltd, Newcastle, U.K). Data processing included the following steps: (i) Features

detection, (ii) Features alignment across all samples, (iii) Volume integration for 2-6 charge-state ions, (iv) Normalization on feature median ratio, (v) Import of sequence information, (vi) Calculation of protein abundance (sum of the volume of corresponding peptides), (vii) A statistical test was performed and proteins were filtered based on p -value <0.05 . Only non-conflicting features and unique peptides were considered for calculation at protein level. Quantitative data were considered for proteins quantified by a minimum of 2 peptides.

The mass spectrometry proteomics data have been deposited to the ProteomeXchange Consortium via the PRIDE (4) partner repository with the dataset identifier PXD021457

Transmission electron microscopy (TEM)

Human biopsies were fixed with 2.5 % (v/v) glutaraldehyde in 0.1M phosphate buffer (pH 7.4) for 1h at room temperature (RT). Then samples were washed in 0.1M phosphate buffer and post-fixed in 1% (v/v) osmium tetroxide in phosphate buffer 0.1 M for 2h in the dark at RT, then were washed in water and dehydrated through a series of graded ethanol and embedded in a mixture of pure ethanol and epoxy resin (Epon 812; Delta Microscopy, Toulouse, France) 50/50 (v/v) for 2 hours and then in 100% resin overnight at RT. Polymerization of the resin was carried out between 24-48 hours at 60 ° C.

Samples were then sectioned using a diamond knife (Diatome, Biel-Bienne, Switzerland) on an ultramicrotome (EM UC7, Leica Microsystems, Vienna, Austria). Ultrathin sections (65 nm) were picked up on copper grids and then stained with uranyl acetate and lead citrate. Grids were examined with a transmission electron microscope (H7650, Hitachi, Tokyo, Japan) at 80kV.

SI Figures:

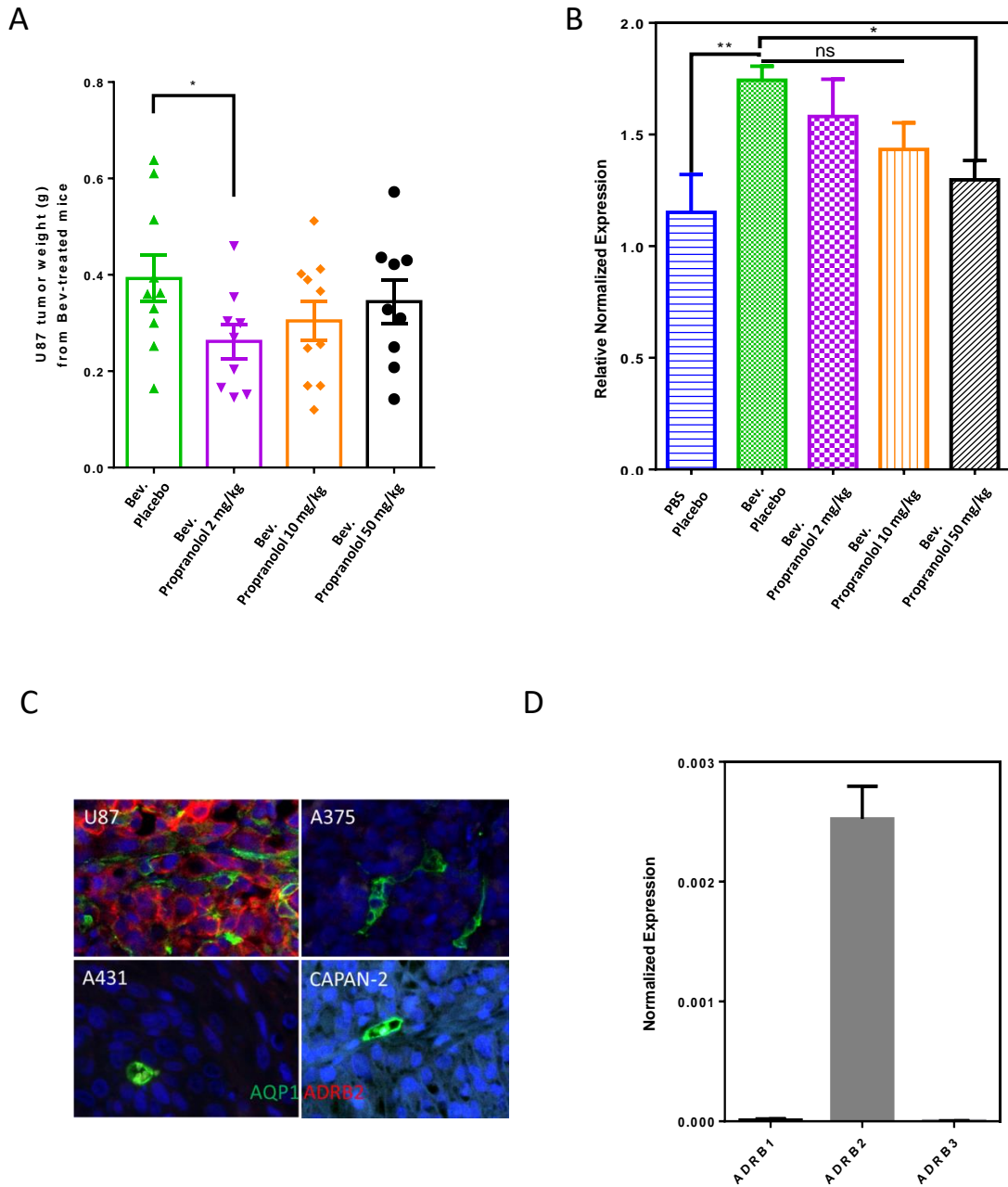


Fig. S1. Propranolol antitumor effect study *in vivo*. A. U87 tumor weight of Bev and non-Bev-treated mice co-treated with 2, 10 or 50 mg/kg of propranolol or placebo. * Bev-treated mice combined with 2 mg/kg of propranolol had significantly smaller tumors compared to Bev-treated mice with placebo ($p=0.0464$). B. VEGF-A expression in U87 tumors measured by human specific qPCR. Bev-treated mice (Avastin) had higher tumor VEGF expression. Inhibitory dose-response was observed but did not correlate with tumor response. C. ADRB2 (red) and AQP1 (green) IHF staining of tumor xenograft from U87, A375, A431, CAPAN-2 human tumor cell lines. D. ADRB1, ADRB2 and ADRB3 expression in U87 cell line measured by qPCR. ADRB2 was the only ADRB gene significantly expressed. * $P<0.05$ ** $P<0.005$

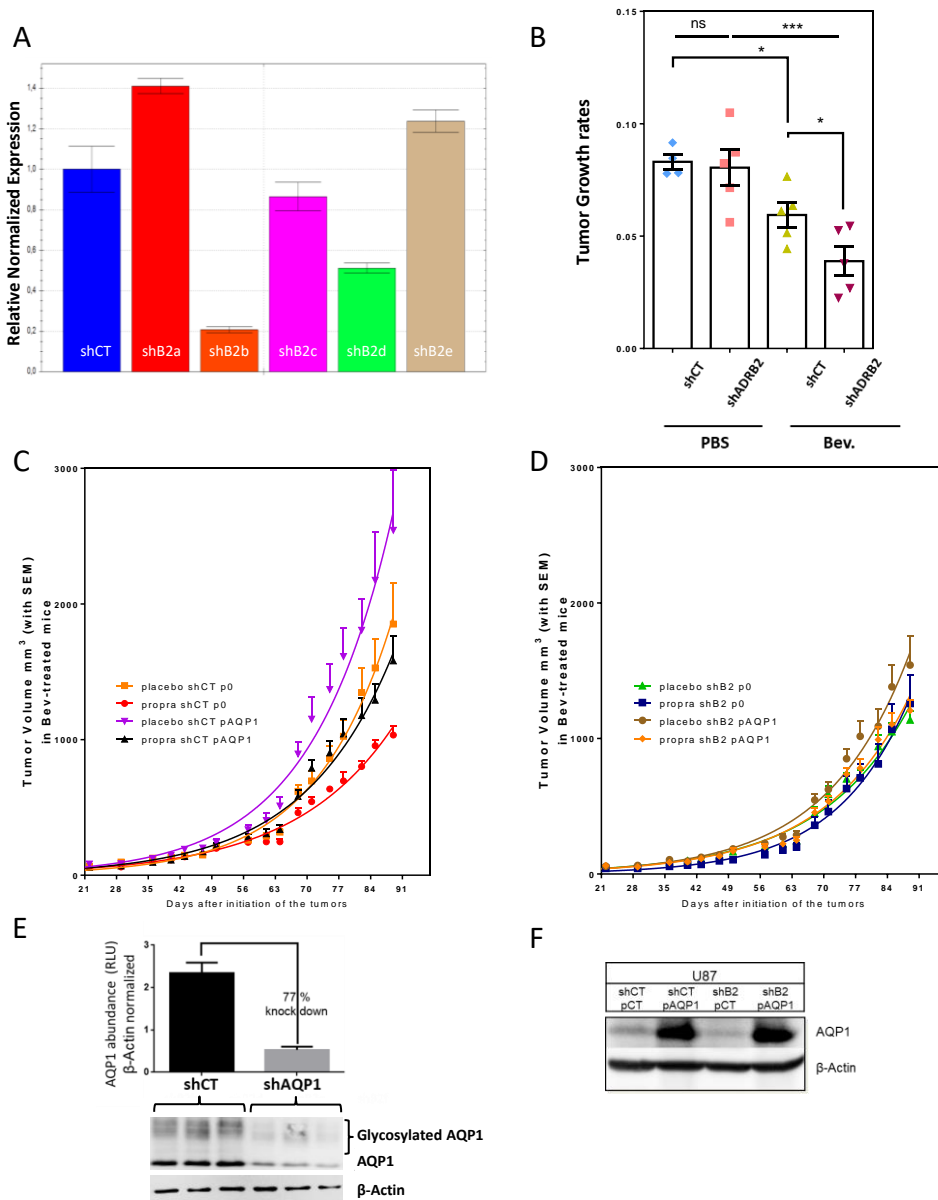


Fig. S2. Betaadrenergic pathway and AQP1 as a target of propranolol in U87 tumors. A. ADRB2 shRNAs efficiency measured by qPCR in U87 shRNA-lentivirus transduced cells. Among 5 different shADRB2, shADRB2b had a satisfactory 75% inhibition effect on ADRB2 mRNA level. **B.** U87shCT and shADRB2 tumors Specific Growth Rate (SGR) in non-Bev and Bev-treated mice was estimated according to the following equation: $SGR = \ln 2 / DT$, in which DT= doubling time. The higher the SGR, the faster the tumors grow. Propranolol significantly inhibit tumor growth speed. * $P < 0.05$ ** $P < 0.005$ *** $P < 0.0005$. **C.** U87 shCT tumor growth with (pAQ1) or without (p0) AQP1 overexpression, in bev-treated mice co-treated with propranolol or placebo. **D.** U87 shADRB2 (shB2) tumor growth with (pAQ1) or without (p0) AQP1 overexpression, in bev-treated mice co-treated with propranolol or placebo. **E.** AQP1 protein RLU quantification normalized by beta-actin show efficient downregulation of AQP1 using shRNA lentiviral vector. AQP1 knockdown is measured by Western-blot on 3 on different extracted U87 tumors from each group (shCT and shAQ1). **F.** AQP1 overexpression in U87 cells using pAQ1 lentiviral construct or pCT as a control, evidenced by western-blot.

NICH: 3 patients
(40X, entire field)

CD34 AQP1

RICH: 3 patients
(40X, entire field)

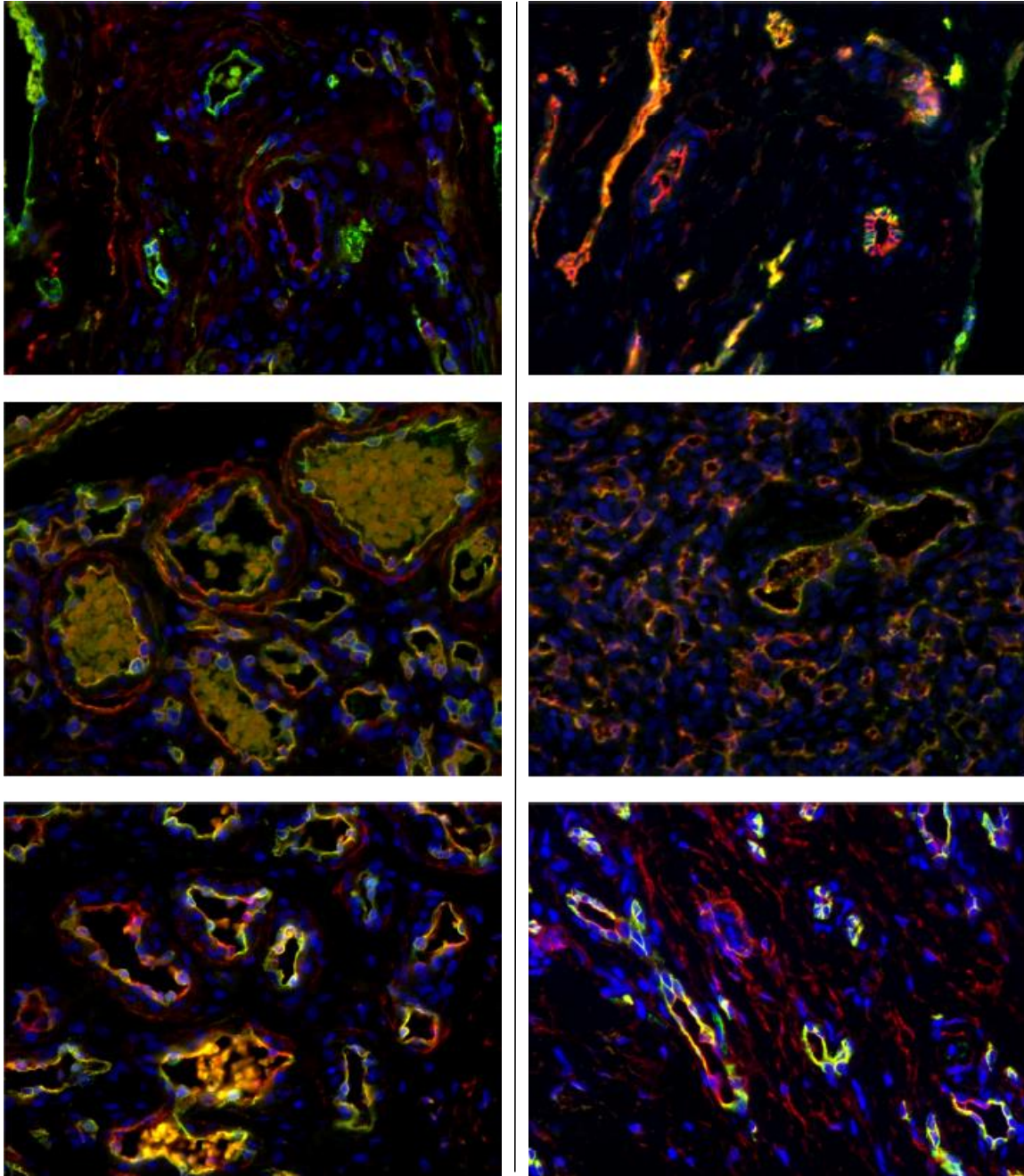


Fig. S3. AQP1/CD34 co-staining by IHC of NICH from 3 patients and RICH from 3 patients (NICH: Non-Involuting Hemangioma; RICH: Rapidly Involuting Hemangioma). Merged image of CD34 (red), AQP1 (green) and DAPI. Lesional ECs are AQP1-positive. Magnification 40X, entire field.

PICH: 6 patients
CD34 AQP1

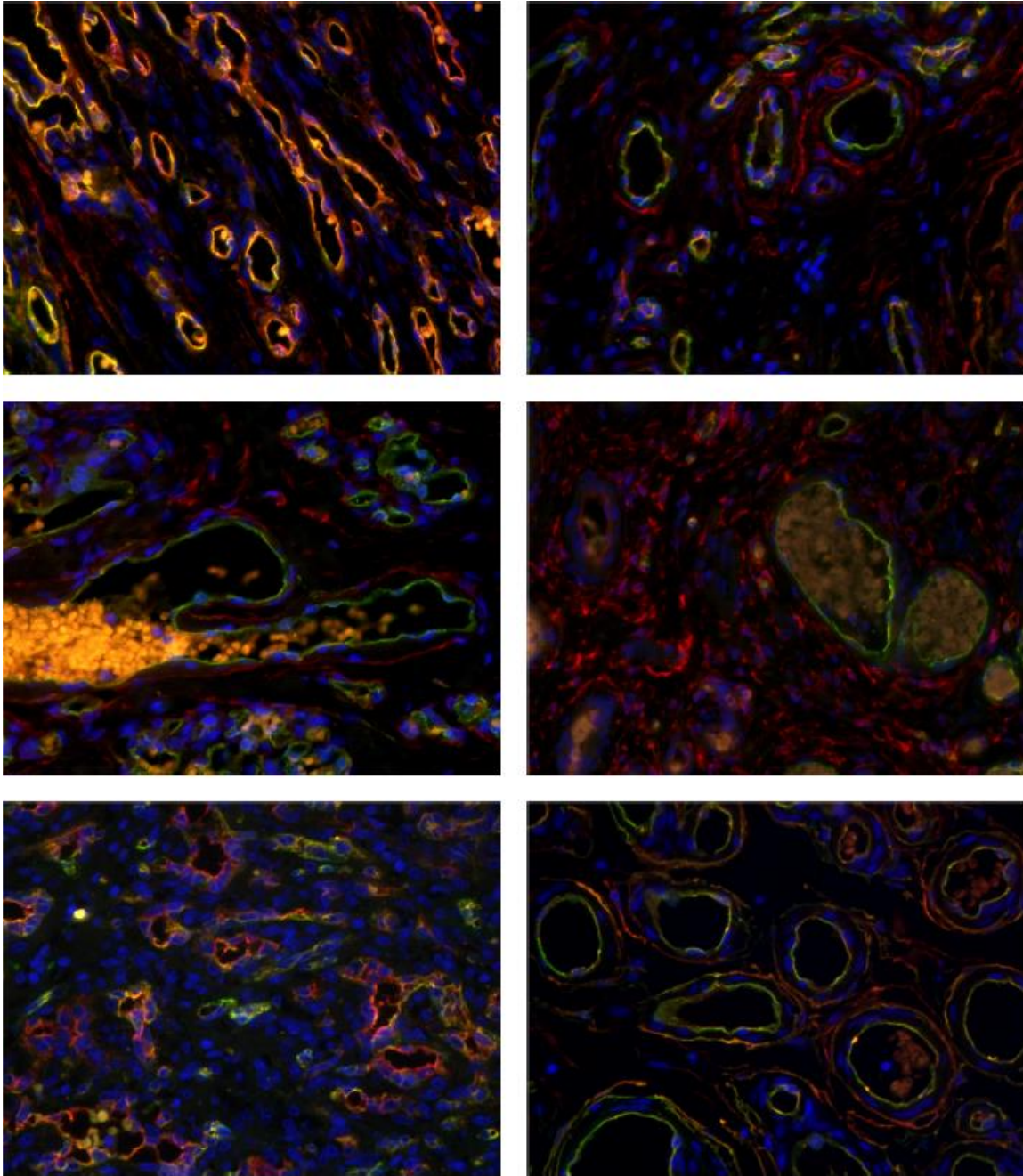


Fig. S4. AQP1/CD34 co-staining by IHF of PICH from 6 patients (PICH: Partially Involute Congenital Hemangioma) Merged image of CD34 (red), AQP1 (green) and DAPI. Lesional ECs are AQP1-positive. Magnification 40X, entire field.

IH: 9 patients

CD34 AQP1

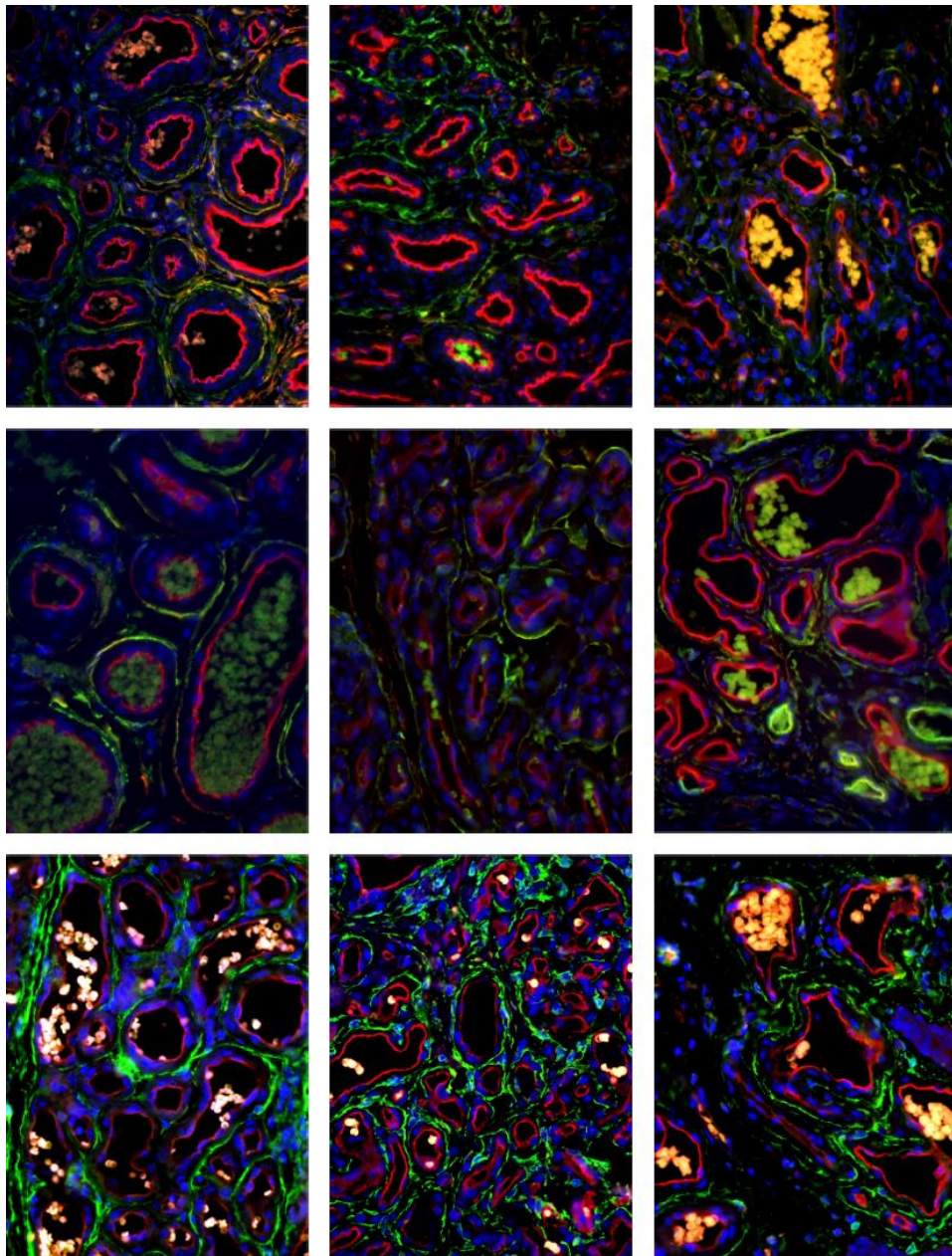
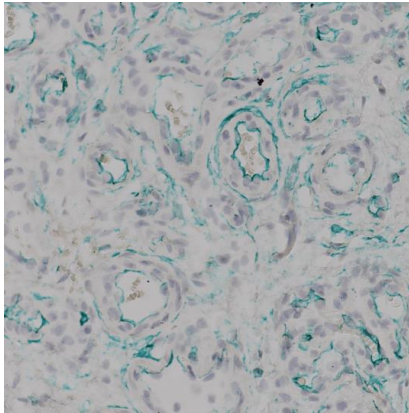


Fig. S5. AQP1/CD34 co-staining by IHF of IH from 9 patients. Merged image of CD34 (red), AQP1 (green) and DAPI. Lesional vessels of IH show a unique AQP1 profile. Magnification 40X.

A IHC staining



CD34 Histogreen

B IHF staining

CD34 AQP1 DAPI

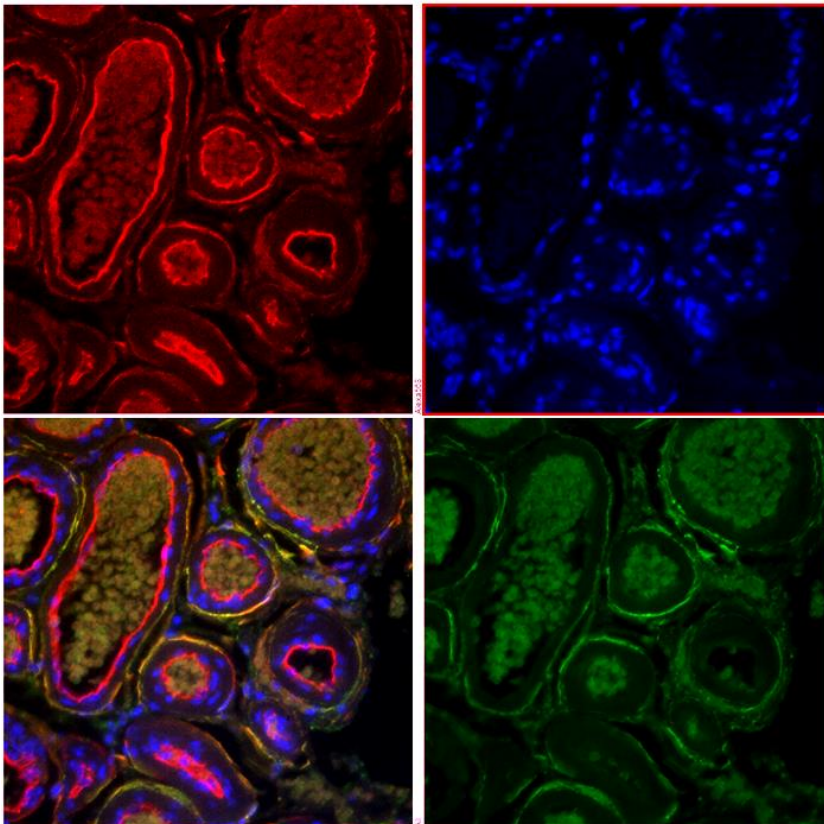


Fig. S6. CD34 positive cells in IH. **A.** CD34 Histogreen IHC staining. **B.** IHF staining with side-by-side, single label for each marker and the merged image of CD34 (red), AQP1 (green) and DAPI, a CD34⁺ railway staining is observed with the inner layer being endothelial cells AQP1⁻ and the outer layer being telocytes AQP1⁺.

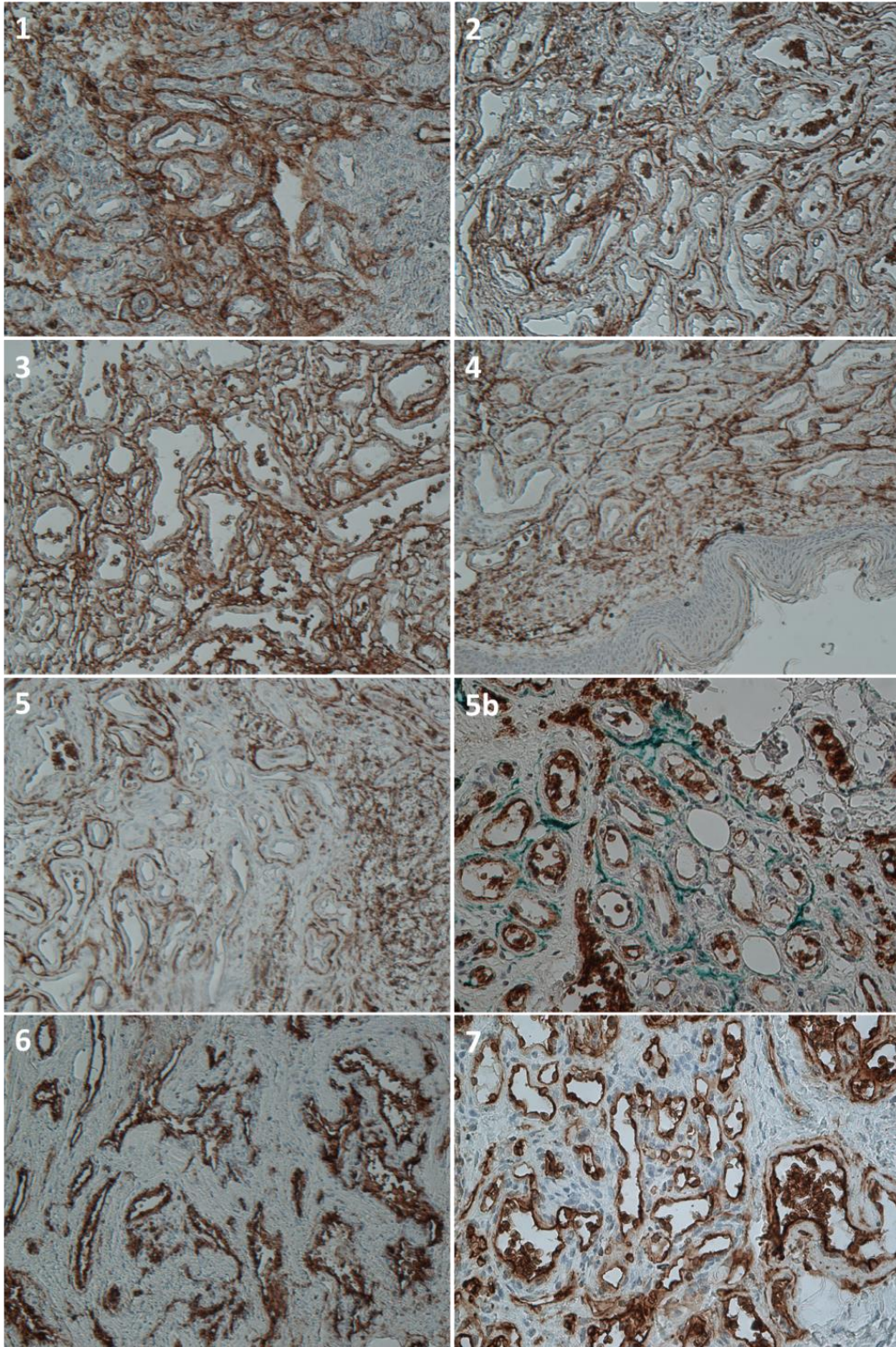


Fig. S7. DAB IHC of AQP1 and blue counterstained nuclei with hematoxylin. 1 to 5 are AQP1 staining of IH patients 1 to 5 respectively, magnification 20X. 5b is IH patient 5 with GLUT1 in DAB (brown) and AQP1 in Histogreen 6 and 7 are NICH patients 1 and 2. (Magnification 40X, entire fields)

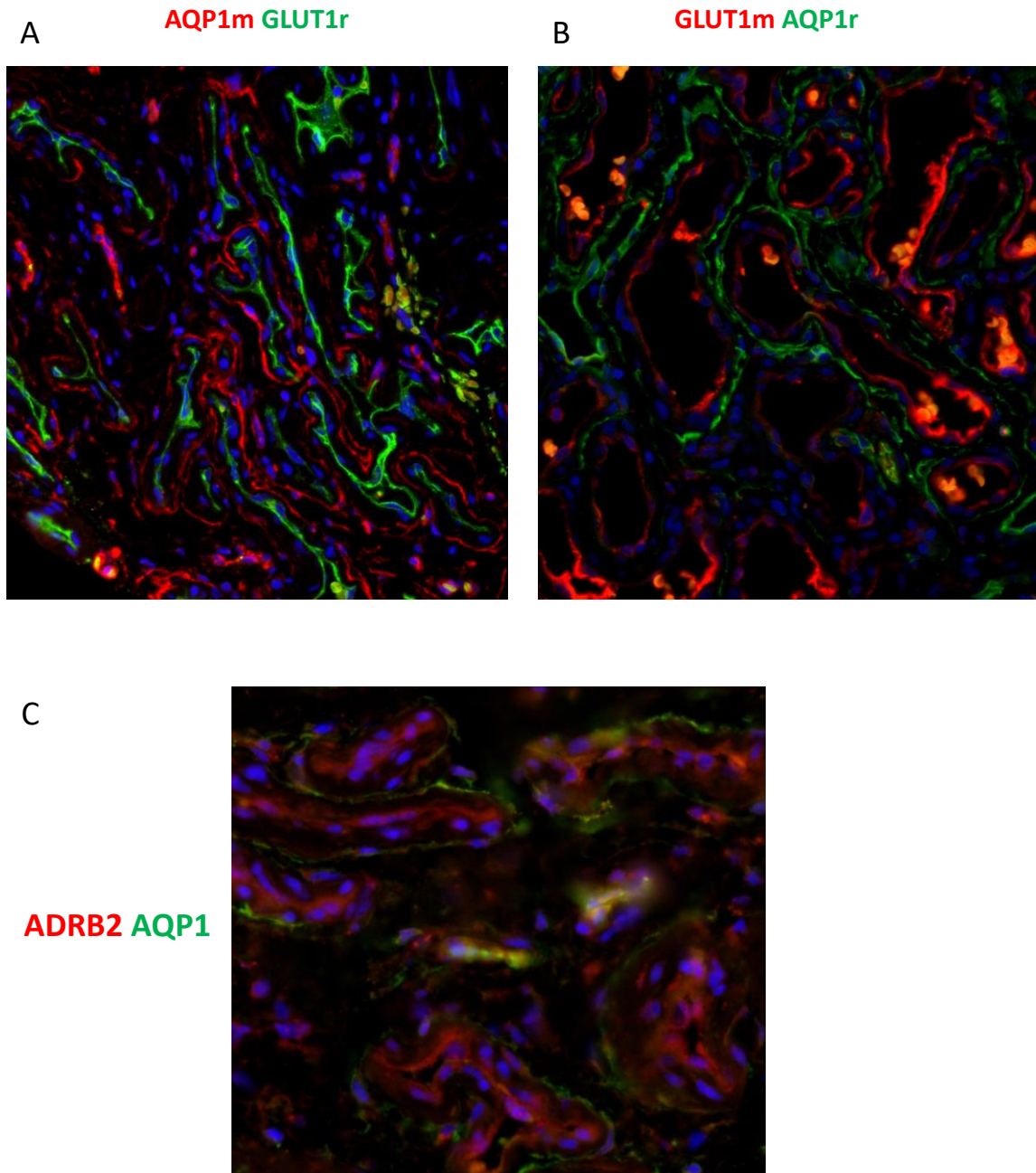


Fig. 8. IHF of IH with AQP1, GLUT1 or ADRB2 stainings **A.** AQP1 mouse monoclonal antibody (red) and GLUT1 rabbit polyclonal (green) compared to **B.** staining with AQP1 rabbit polyclonal antibody (green) and GLUT1 mouse monoclonal (red) rabbit (green). Staining and specificity of antibodies were validated. **C.** ADRB2 (red) AQP1 (green) co-staining. Magnification 40X.

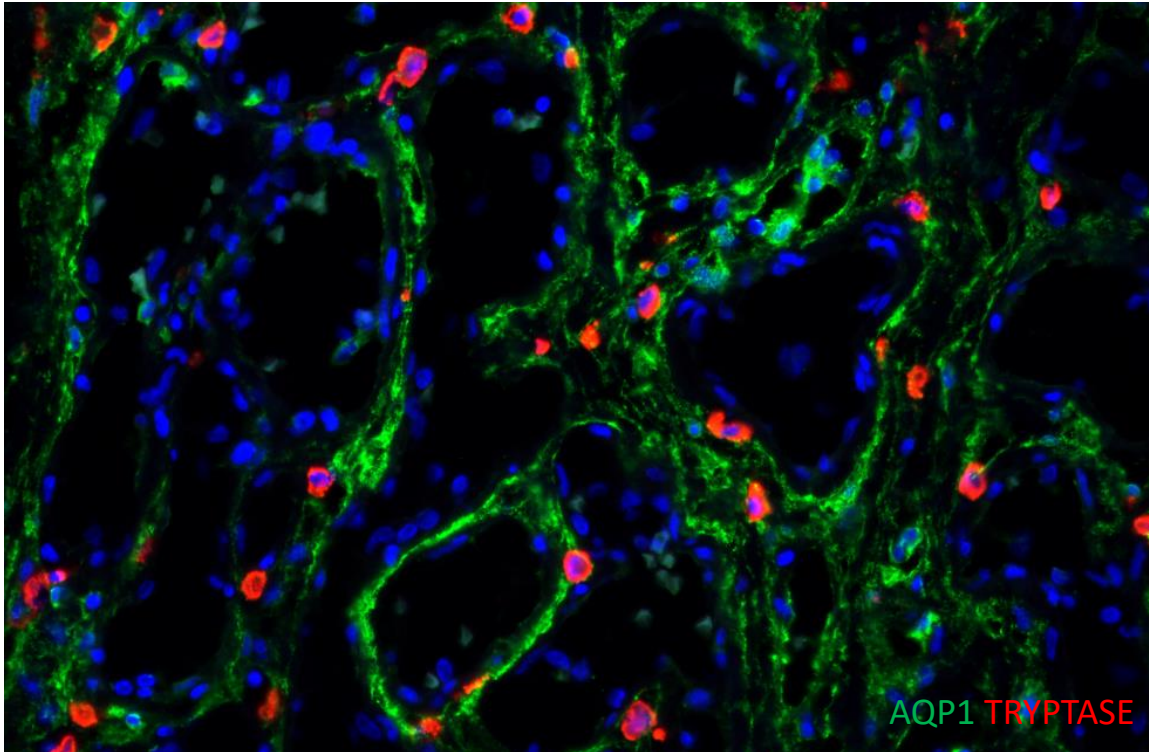
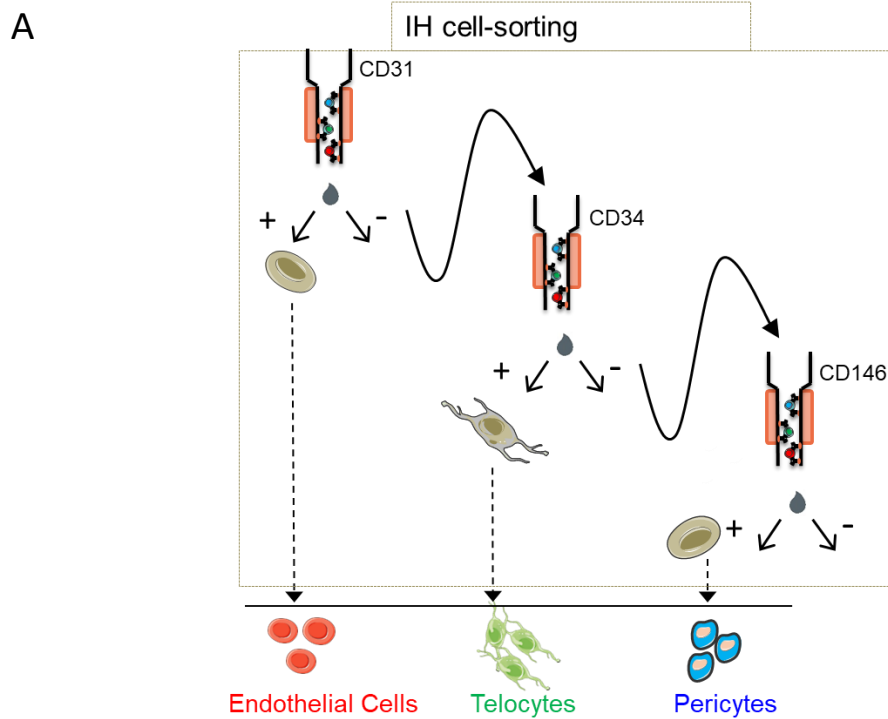


Fig. S9. Mast cells are in close contact with telocytes. Tryptase-positive mast cells (in red) are in direct contact with AQP1-positive telocytes (green). (Magnification 40X, entire fields)



B CD34 immunodetection

C CD146 immunodetection

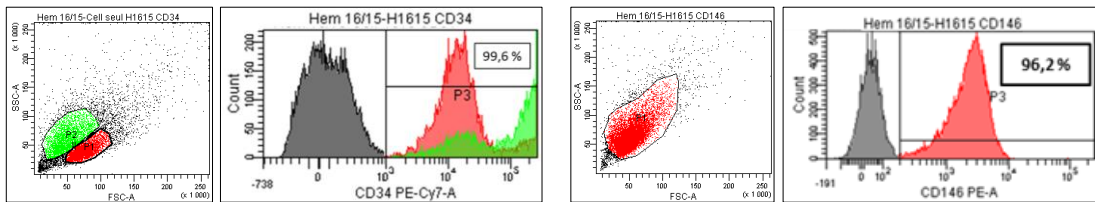


Fig. S10. IH fresh tissue cell sorting for in vitro culture, labelling and assays. **A.** Sequential cell sorting with magnetic bead coupled antibodies directed to CD31, CD34, CD146. **B.** Cytometry quality control for CD34+ cells, example of a single CD34 cell sorting from IH tissue. Here, CD34 sorting was done before CD31, so two CD34+ populations were identified. Then CD31 sorting was always done before CD34 sorting, in order to separate EC before TC sorting. **C.** Cytometry quality control for CD146+ cells (pericytes fraction).

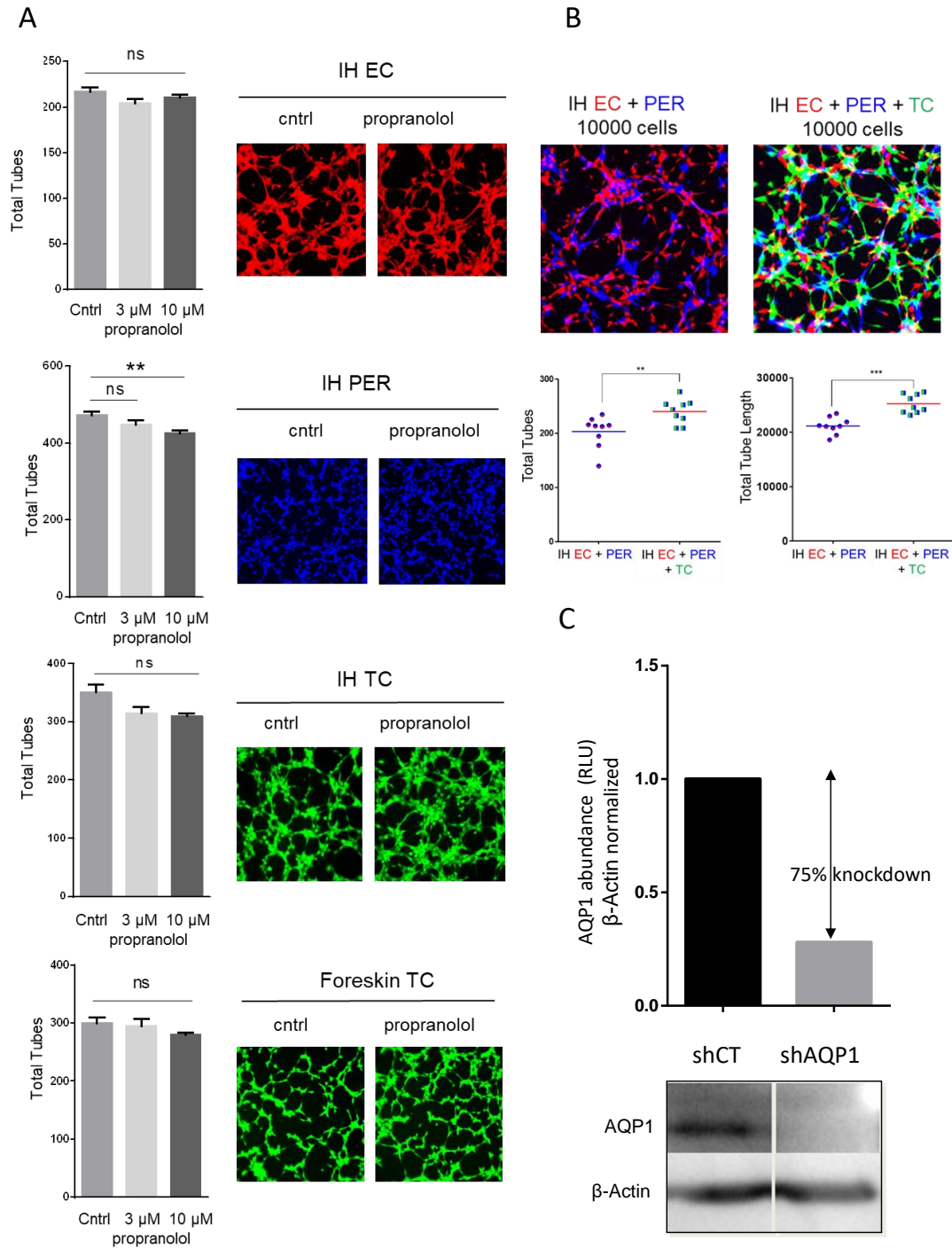


Fig. S11. Separated cell-type tubulogenesis assay and shAQP1 efficiency in IH-TC. A. Propranolol has no major effect on tubulogenic properties of IH-EC, IH-PER and IH-TC in vitro. IH cells were labeled with three different fluorescent dyes, EC in red, TC in green, PER in blue. When IH-EC, IH-PER and IH-TC cells were used separately in tubulogenesis assay, no major effect of propranolol on tubulogenic properties of each of the 3 IH-cells or control foreskin-TC were found. **B.** shAQP1 efficiency in IH-TC by western-blot on protein extracted from transduced IH-TC using shCT and shAQP1. AQP1 protein RLU quantification normalized by beta-actin show efficient knockdown of AQP1 using shAQP1 lentiviral vector compared to shCT.

Table S1. Proteins differentially expressed between xenografts treated with Bev vs PBS as well as the combination of Bev and propranolol vs Bev alone.

Protein name	Bev vs PBS				(Bev+Propranolol) vs (Bev+Placebo)			
	Peptides used for quantitation	Confidence score	Anova (p)	Fold Change	Peptides used for quantitation	Confidence score	Anova (p)	Fold Change
Retinoic acid receptor responder protein 2 (RARRES2)	2	6.05	4.35E-02	34.49	2	6.05	8.60E-01	-2.17
Immunoglobulin kappa constant (IGKC)	7	40.97	4.31E-02	7.83	7	40.97	1.39E-01	2.17
Amine oxidase [flavin-containing] B (MAOB)	2	5.93	8.10E-02	4.38	2	5.93	2.05E-02	-14.29
C-type lectin domain family 11 member A (CLEC11A)	4	11.44	4.00E-03	3.69	4	11.44	8.39E-02	-1.89
Immunoglobulin heavy constant gamma 1 (IGHG1)	6	44.61	8.79E-03	3.57	6	44.61	1.70E-01	1.60
Adenylosuccinate synthetase isozyme 1 (ADSSL1)	3	12.29	3.17E-02	3.17	3	12.29	6.24E-01	-1.27
Aquaporin-1 (AQP1)	4	20.13	4.86E-02	3.04	4	20.13	9.41E-03	-2.33
Collagen alpha-1(I) chain (COL1A1)	8	31.85	2.73E-02	3.02	8	31.85	4.76E-02	-2.04
Stromelysin-2 (MMP10)	3	7.39	2.45E-02	2.45	3	7.39	4.04E-01	-1.12
Laminin subunit alpha-5 (LAMA5)	9	33.15	4.73E-02	2.37	9	33.15	9.49E-01	1.29
72 kDa type IV collagenase (MMP2)	7	20.39	1.10E-01	2.10	7	20.39	4.88E-02	-2.08
CDP-diacylglycerol-inositol 3-phosphatidyltransferase (CDIPT)	4	18.69	2.78E-01	2.07	4	18.69	4.78E-02	-3.13
Acetolactate synthase-like protein	2	6.46	2.91E-01	1.84	2	6.46	1.10E-02	-2.27
Carbonic anhydrase 9 (CA9)	4	13.61	3.48E-02	1.84	4	13.61	5.92E-01	-1.12
Sulfotransferase 1A4 (SULT1A4)	3	9.96	9.34E-01	1.52	3	9.96	4.39E-02	-10.00
Inosine triphosphate pyrophosphatase (ITPA)	5	15.22	3.35E-01	1.38	5	15.22	3.98E-02	-2.17
E3 ubiquitin/ISG15 ligase TRIM25 (TRIM25)	2	6.13	7.65E-01	1.04	2	6.13	3.00E-02	-2.27
Discoidin, CUB and LCCL domain-containing (DCBLD2)	2	5.29	7.17E-01	-1.04	2	5.29	4.39E-02	-2.86
UDP-N-acetylhexosamine pyrophosphorylase (UAP1)	2	9.77	9.66E-01	-1.04	2	9.77	4.58E-02	2.00
Protein FAM136A (FAM136A)	2	4.32	7.17E-01	-1.25	2	4.32	3.10E-03	2.56
Myosin-8 (MYH8)	4	252.28	2.43E-01	-1.39	4	252.28	3.10E-02	2.64
Hemoglobin subunit beta (HBB)	4	25.11	1.62E-01	-1.89	4	25.11	2.69E-02	3.47
Hemoglobin subunit alpha (HBA1)	7	24.48	1.49E-01	-1.89	7	24.48	3.26E-02	3.78
Small nuclear ribonucleoprotein F (SNRPF)	2	7.56	1.04E-02	-2.08	2	7.56	1.67E-01	1.37
Haptoglobin-related (HPR)	2	3.77	1.37E-02	-2.17	2	3.77	1.49E-01	-1.54
Zinc finger CCH-type antiviral protein 1 (ZC3HAV1)	4	14.60	1.89E-02	-2.27	4	14.60	8.25E-01	-1.04
Sulfide:quinone oxidoreductase, mitochondrial (SQOR)	3	16.30	9.28E-02	-2.27	3	16.30	4.70E-02	2.40
Rab3 GTPase-activating protein non-catalytic subunit (RAB3GAP2)	2	7.04	1.84E-03	-2.38	2	7.04	4.12E-03	1.80
Inter-alpha-trypsin inhibitor heavy chain H3 (ITIH3)	7	26.82	4.00E-02	-2.56	7	26.82	9.69E-02	-1.64
Inter-alpha-trypsin inhibitor heavy chain H4 (ITIH4)	7	16.98	2.39E-02	-2.56	7	16.98	2.33E-01	1.25
PDZ domain-containing protein GIPC1 (GIPC1)	2	6.65	2.84E-02	-3.03	2	6.65	4.22E-01	-1.39
Carnitine O-palmitoyltransferase 1 (CPT1A)	4	9.08	4.22E-02	-4.55	4	9.08	1.42E-01	2.18

Table S2. GLUT1 and AQP1 Lesional vascular profiles

	Age (years)	Lesional vascular profile			treated
		Endothelial Cells		Telocytes	
		GLUT1	AQP1	AQP1	
Congenital Hemangiomas NICH PICH RICH	<1	-	+	-	-
	5	-	+	-	-
	8	-	+	+/-	-
	<1	-	+	-	-
	<1	-	+	-	-
	1	-	+	+/-	-
	6	-	+	-	-
	12	-	+	+/-	-
	<1	-	+	-	-
	3	-	+	-	-
	3	-	+	-	-
	1	-	+	-	-
	1	-	+	-	-
9	-	+	+	-	
Infantile Hemangiomas	3	+	-	+	-
	7	+	-	+	-
	<1	+	-	+	-
	2	+	-	+	-
	3	+	-	+	-
	6	+	-	+	-
	1	+	-	+	-
	1	+	-	+	-
	5	+	-	+	-
	10	+	-	+	-
	3	+	-	+	-
	5	+	-	+	-
	8	+	-	+	-
	<1	+	-	+	-
	4	+	-	+	-
	6	+	-	+	-
	<1	+	-	+	-
	9	+	-	+	-
	<1	+	-	+	-
	5	+	-	+	-
	<1	+	-	+	timolol
	<1	+	-	+	timolol
	<1	+	-	+	timolol
	1	+	-	+	timolol
	1	+	-	+	timolol
	3	+	-	+	Propranolol
	<1	+	-	+	Propranolol
	<1	+	-	+	Propranolol
	2	+	-	+	Propranolol
	3	+	-	+	Propranolol
3	+	-	+	Propranolol	
9	+	-	+	Propranolol	
5	+	-	+	Propranolol	
2	+	-	+	Propranolol	
<1	+	-	+	Propranolol	
2	+	-	+	Propranolol	
Dermis		-	+	-	

Table S3. Antibodies

Antibody	Provider	Reference	IHF dilution	WB dilution
AQP1	Merck	AB2219	1/1000	1/500
AQP1	Santa Cruz Biotechnology	sc-25287	1/50	
CD34	Thermofisher	MA1-10202	1/500	
PDGFRa	Abcam	Ab61219	1/500	
c-kit	Santa Cruz Biotechnology	sc-393910	1/50	
vimentin	Dako	M0725	1/200	
α SMA	Abcam	ab7817	1/500	
GLUT-1	Merck	MABS132	1/500	
GLUT-1	Thermofisher	pa1-21041	1/100	
ADRB2	Abcam	ab61778	1/100	
ADRB2	Santa Cruz Biotechnology	sc-271322	1/50	
CAV-1	Santa Cruz Biotechnology	sc-53564	1/50	
Tryprase	Abcam	ab81703	1/2000	
CD68	Dako	M0876	1/100	
CD133	Merck	MAB4399-I	1/50	
CD168	Abcam	ab224768	1/100	
Ki-67	Vectorlabs	VP-K452	1/200	
VEGF-A	Abcam	ab1316	1/100	
β -Actin	Sigma-Aldrich	A2228		1/4000
Horse Anti-Mouse HRP	Vectorlabs	PI-2000		1/5000
Goat Anti-Rabbit HRP	Vectorlabs	PI-1000		1/2000
Goat Anti-Rabbit 488	Abcam	ab150077	1/500	
Goat Anti-Rabbit 555	Abcam	ab 150078	1/500	
Goat Anti-Mouse 488	Abcam	ab150113	1/500	
Goat Anti-Mouse 555	Abcam	ab150114	1/500	
Donkey Anti-Rabbit 568	Abcam	ab175470	1/500	
Donkey Anti-Mouse 568	Abcam	ab175472	1/500	

SI References

1. M. Hosseini, *et al.*, Premature Skin Aging Features Rescued by Inhibition of NADPH Oxidase Activity in XPC-Deficient Mice. *J. Invest. Dermatol.* **135**, 1108–1118 (2015).
2. M. Hosseini, *et al.*, Energy Metabolism Rewiring Precedes UVB-Induced Primary Skin Tumor Formation. *Cell Rep.* **23**, 3621–3634 (2018).
3. L. Käll, J. D. Canterbury, J. Weston, W. S. Noble, M. J. MacCoss, Semi-supervised learning for peptide identification from shotgun proteomics datasets. *Nat. Methods* **4**, 923–925 (2007).
4. Perez-Riverol Y, Csordas A, Bai J, Bernal-Llinares M, Hewapathirana S, Kundu DJ, Inuganti A, Griss J, Mayer G, Eisenacher M, Pérez E, Uszkoreit J, Pfeuffer J, Sachsenberg T, Yilmaz S, Tiwary S, Cox J, Audain E, Walzer M, Jarnuczak AF, Ternent T, Brazma A, Vizcaíno JA. The PRIDE database and related tools and resources in 2019: improving support for quantification data. *Nucleic Acids Res* **47**(D1):D442-D450 (2019).